Cross sections of α-induced reactions slightly below doubly magic ^{40}Ca from the statistical model

P. Mohr, R. Talwar, and M. L. Avila

Phys. Rev. C **98**, 045805 — Published 25 October 2018

DOI: 10.1103/PhysRevC.98.045805

Cross sections of α-induced reactions slightly below doubly-magic ^{40}Ca from the statistical model

P. Mohr*
Diakonie-Klinikum, Schwäbisch Hall D-74523, Germany and
Institute for Nuclear Research (Atomki), Debrecen H-4001, Hungary

R. Talwar and M. L. Avila
Physics Division, Argonne National Laboratory, Argonne, IL 60439 USA
(Dated: September 2, 2018)

New experimental data for the ^{38}Ar(α,n)^{41}Ca and ^{38}Ar(α,p)^{41}K reactions were used to find a best-fit set of parameters for statistical model calculations. The very good agreement between the experimental data and the best-fit calculation confirms the applicability of the statistical model for nuclei in the vicinity of the doubly-magic ^{40}Ca despite of their relatively low level densities. The present study investigates the sensitivities and finds that the α-nucleus and the nucleon-nucleus potentials are the most important ingredients for the calculation of (α,n) and (α,p) reactions in the statistical model. Furthermore, the width fluctuation correction plays an essential role in the peculiar case of ^{38}Ar. The best-fit parameters from ^{38}Ar are applied to the mirror nucleus ^{38}Ca and the neighboring ^{36}Ar and ^{40}Ar nuclei. For ^{38}Ca this results in an astrophysical reaction rate of the ^{38}Ca(α,p)^{41}Sc reaction which has a flatter temperature dependence compared to all previous calculations. For ^{40}Ar a better reproduction of ^{40}Ar(α,p)^{43}K data from literature is obtained. The disagreement between calculation and an early experimental data point for the ^{36}Ar(α,p)^{39}K reaction persists.

I. INTRODUCTION

The cross sections and stellar reaction rates of α-induced reactions play an important role in various astrophysical scenarios. For targets slightly below the doubly-magic ^{40}Ca, the ^{38}Ar(α,p)^{41}K and ^{38}Ar(α,n)^{41}Ca reactions have been studied recently because their reverse ^{41}K(p,α)^{38}Ar and ^{41}Ca(n,α)^{38}Ar reactions have been identified to affect the abundance of the relatively short-lived ^{41}Ca nucleus in the early solar system. The dedicated experiment has provided several (α,p) and (α,n) cross sections at low energies (see [1] and references therein). Furthermore, (α,p) reactions on isospin $T_z = -1$ nuclei like ^{30}S [2, 3], ^{34}Ar [4, 5], and ^{38}Ca play a key role in the so-called αp-process in X-ray bursters [6–8]. Obviously, direct experiments on these short-lived $T_z = -1$ nuclei are very difficult, and often indirect information from (p,t) reactions is used to estimate the stellar reaction rates [3, 4, 9].

In general, a very reasonable description of α-induced reaction cross sections at low energies has been found for nuclei in the $A \approx 20 - 50$ mass range [10]. It is based on the statistical model (StM) in combination with the widely used simple 4-parameter α-nucleus optical model potential (A-OMP) by McFadden and Satchler [11]. Interestingly, further ingredients of the StM play a very minor role in this mass range because the A-OMP defines the total α-induced reaction cross section $\sigma_{\rm reac}$ which is typically dominated by either the (α,n) or the (α,p) channel. However, the simple approach of a dominating (α,n) or (α,p) channel does not hold in vicinity of the doubly-magic ^{40}Ca. The Q-values of the ^{38}Ar(α,n)^{41}Ca and ^{38}Ar(α,p)^{41}K reactions are both significantly negative, and thus the description of these reactions in the StM requires additional care.

It is the scope of the present paper to present the relevant details and improvements of the StM calculations in [1] for the ^{38}Ar(α,n)^{41}Ca and ^{38}Ar(α,p)^{41}K reactions. In addition, these improvements will be used to predict α-induced cross sections for the mirror nucleus ^{38}Ca and for ^{36}Ar and ^{40}Ar. For the latter two argon isotopes significant discrepancies between the StM calculations and very old experimental data [12] were identified in [10]. Note that new experimental data for the two further outliers in [10], ^{23}Na [13–15] and ^{33}S [16] (see also [17]), supersede previous data [18, 19] and are now in better agreement with the earlier predictions in [10].

II. α-INDUCED CROSS SECTIONS IN THE STATISTICAL MODEL FOR TARGETS CLOSE TO ^{40}CA

A. General remarks

The cross sections of α-induced reactions in the present study have been calculated within the StM. By definition, the StM provides average cross sections which are based on the assumption of a sufficiently high level density in the compound nucleus. In the following, the compound nucleus ^{42}Ca and the system ^{38}Ar+α with the ^{38}Ar(α,n)^{41}Ca and ^{38}Ar(α,p)^{41}K reactions have been chosen as an example.

In reality, the (α,n) and (α,p) cross sections for targets

* Electronic Address: mohr@atomki.mta.hu

close to ^{40}Ca are composed of the contributions of several resonances which may be broad and overlapping. A typical experiment averages these resonance contributions over an energy interval ΔE which is essentially defined by the energy distribution of the beam and the energy loss of projectiles in the target:

$$\Delta E = E^{\rm exp}_{\rm max} - E^{\rm exp}_{\rm min} \quad (1)$$

with $E^{\rm exp}_{\rm max}$ and $E^{\rm exp}_{\rm min}$ being the highest and lowest experimental energy (given as $E_{\rm c.m.}$ in the center-of-mass system). This experimental energy window ΔE corresponds to a window ΔE^* in excitation energies E^* in the compound nucleus from $E^*_{\rm min} = Q_\alpha + E^{\rm exp}_{\rm min}$ to $E^*_{\rm max} = Q_\alpha + E^{\rm exp}_{\rm max}$ with the Q-value Q_α of the (α,γ) reaction.

Depending on the experimental conditions, ΔE may be of the order of a few keV (for primary beams and thin targets) or much larger (typically a few hundred keV for secondary and/or radioactive ion beams with low intensities and the required thick targets). Obviously, for a successful application of the StM a sufficient number of resonances has to be located within the experimental energy interval ΔE. Otherwise, the StM is only able to provide the average trend of the experimental data.

Besides theoretical estimates from level density formulae, there is a simple experimental criterion for the applicability of the StM. As long as the excitation functions of the (α,n) and (α,p) reactions show a relatively smooth energy dependence, the application of the StM should be justified. Contrary, the StM must fail to reproduce experimental excitation functions where the data points show significant scatter from the contributions of individual resonances. The new experimental data for the chosen examples ^{38}Ar(α,n)^{41}Ca and ^{38}Ar(α,p)^{41}K [1] show a relatively smooth energy dependence (except the two lowest data points of the (α,p) reaction), and thus the StM should be applicable in the present case although the level densities in the semi-magic ^{38}Ar ($N = 20$) target nucleus and ^{42}Ca ($Z = 20$) compound nucleus remain relatively small.

B. Formalism of the statistical model

The Hauser-Feshbach StM [20] is described in many publications. A detailed description for its application to low-energy reactions and the calculation of astrophysical reaction rates is provided e.g. in [21]. Here we briefly repeat the essential definitions which are relevant in the following discussion.

In a schematic notation the reaction cross section in the Hauser-Feshbach (HF) StM [20] is proportional to

$$\sigma(\alpha, X)_{\rm HF} \sim \frac{T_{\alpha,0} T_X}{\sum_i T_i} = T_{\alpha,0} \times b_X \quad (2)$$

with the transmission coefficients T_i into the i-th open channel and the branching ratio $b_X = T_X / \sum_i T_i$ for the decay into the channel X. The total transmission is given by the sum over all contributing channels: $T_{\rm tot} = \sum_i T_i$. The T_i are calculated from optical potentials for the particle channels and from the gamma-ray strength function for the photon channel. The T_i include contributions of all final states j in the respective residual nucleus in the i-th exit channel. In practice, the sum over all final states j is approximated by the sum over low-lying excited states up to a certain excitation energy $E_{\rm LD}$ (these levels are typically known from experiment) plus an integration over a theoretical level density for the contribution of higher-lying excited states:

$$T_i = \sum_j T_{i,j} \approx \sum_j^{E_j < E_{\rm LD}} T_{i,j} + \int_{E_{\rm LD}}^{E_{\rm max}} \rho(E)\, T_i(E)\, dE \quad (3)$$

$T_{\alpha,0}$ in Eq. (2) refers to the entrance channel with the target nucleus (^{38}Ar in the present example) in the ground state and defines the total α-induced reaction cross section $\sigma_{\rm reac}$. (For the calculation of astrophysical reaction rates, thermally excited states in the target have to be considered in addition.)

There are correlations between the incident and outgoing waves which have to be taken into account by a so-called width fluctuation correction factor (WFCF) $W_{\alpha X}$:

$$\sigma(\alpha, X) = \sigma(\alpha, X)_{\rm HF} \times W_{\alpha X} \quad (4)$$

The WFCFs approach unity at higher energies as soon as many reaction channels are open. At low energies the WFCFs lead to an enhancement of the compound-elastic cross section and to a reduction of the (α,X) reaction cross sections. Several methods have been suggested to calculate these WFCFs (see further discussion below).

C. Ingredients of the statistical model and sensitivities

From Eqs. (2)–(4) it is obvious that the calculated cross sections in the StM depend on the transmissions T_i which in turn depend on the following ingredients. The neutron and proton transmissions T_n and T_p are calculated from nucleon optical model potentials (N-OMP); the α transmission T_α depends on the chosen α-nucleus optical model potential (A-OMP), and the γ transmission T_γ is given by the γ-ray strength function (GSF). Note that other channels are typically closed at low energies (or have only very minor contributions).

All transmissions T_n, T_p, T_α, and T_γ have a further implicit dependence on the chosen level density (LD) which results from Eq. (3); $T_{\alpha,0}$ in Eq. (2) is independent of the chosen LD. For completeness we point out that the choice of a LD in Eq. (3) should not be confused with the required sufficiently high LD in the energy interval ΔE in Eq. (1). The former is a choice for a calculation; the latter is the basic prerequisite for the applicability of the

StM; as such, it is a physical property of the system under investigation and cannot be chosen or even changed in calculations.

Summarizing, the cross section in the StM depends explicitly on the chosen A-OMP, N-OMP, and GSF, and implicitly on the chosen LD. As will be shown, the A-OMP is the most important parameter, whereas the remaining parameters N-OMP, GSF, and LD have relatively minor influence on the (α,n) and (α,p) cross sections. Typically, the (α,γ) cross section is sensitive to a combination of all parameters as soon as the energy exceeds the (α,n) or (α,p) threshold.

In recent work, two different approaches have been followed to study the sensitivities of the calculated cross sections in the StM. A strictly mathematical definition for the sensitivity is for example provided in [22]. Eq. (1) of [22] defines a relative sensitivity of 1.0 if a variation of the input parameter (typically, a transmission T_i) by a certain factor (e.g., a factor of two) leads to a variation of the resulting cross section by the same factor. A more empirical approach was followed in [1, 23]. Here a reasonable variation of the input parameters T_i was estimated from the choice of different parametrizations (e.g., a reasonable variation of T_α was estimated from the choice of different A-OMPs), and finally a χ^2-based assessment was used to select combinations of A-OMPs, N-OMPs, GSFs, and LDs. These χ^2-selected combinations are able to reproduce the available experimental data within the measured energy range and should be used for the prediction of cross sections outside the measured energy range with improved reliability. Although the method of both approaches is different, the conclusions for the reactions under study in the present work are practically identical.

The last ingredient of the StM calculations is the chosen method for the calculation of the WFCFs in Eq. (4). Typically, for α-induced reactions the importance of the WFCFs is very minor. However, this typical behavior does not apply for the α-induced reactions on ^{38}Ar, and thus the WFCFs have to be taken into account for ^{38}Ar and neighboring target nuclei.

As studied in detail in the mass range $20 \leq A \leq 50$, a more or less generic behavior of α-induced reaction cross sections is found [10]. As soon as either the (α,n) or (α,p) particle channel is open, this channel typically dominates: $T_{\alpha,0} \ll T_n$ or T_p, and thus the branchings b_n or b_p approach unity, see Eq. (2). This is obvious for the neutron channel because of the missing Coulomb barrier; but it holds also for the proton channel because the Coulomb barrier in the proton channel is much lower than in the α channel. Consequently, either the (α,p) or (α,n) channel contributes with typically 90% or more to $\sigma_{\rm reac}$ [10]. Under these conditions the WFCFs for the (α,X) channels become negligible because even a dramatic enhancement of the weak compound-elastic channel, e.g. say $W_{\alpha\alpha} = 2$, does practically not affect and reduce the dominating (α,p) or (α,n) cross sections.

For ^{38}Ar the Q-values for the typically dominating (α,n) or (α,p) channels are both significantly negative ($Q_{\rm n} = -5.22$ MeV and $Q_{\rm p} = -4.02$ MeV). As a consequence, the usual approximation $T_{\alpha,0} \ll T_n$ or T_p does not hold for ^{38}Ar, and after formation of the compound nucleus ^{42}Ca, it may also decay back to the α channel (compound-elastic channel). As the WFCFs enhance this channel and reduce the (α,n) and (α,p) channels, it is important to study different methods for the calculation of the WFCFs.

The results in the following sections are based on calculations with the widely used code TALYS, version 1.80, [24] which provides the choice of different A-OMPs, N-OMPs, GSFs, LDs, and methods for the calculation of WFCFs. In addition, the code has been modified to implement the recently suggested A-OMP ATOMKI-V1 for heavy targets ($A \gtrsim 90$) [25]. In Sect. III a detailed study of the sensitivies is provided for the target nucleus ^{38}Ar. The results for ^{38}Ar are used to constrain the parameters for the mirror nucleus ^{38}Ca and for the neighboring isotopes ^{36}Ar and ^{40}Ar in Sect. IV.

III. RESULTS FOR ^{38}AR

A χ^2 search has been performed to find the best combination of input parameters for the new ^{38}Ar(α,n)^{41}Ca and ^{38}Ar(α,p)^{41}K data [1]. As already summarized in [1], the best-fit parameters consist of the A-OMP by McFadden and Satchler [11] and the TALYS-default N-OMP by Koning and Delaroche [26]. The χ^2 search is not very sensitive to the chosen LD, but the smallest χ^2 is found for the LD calculated from the generalized superfluid model [27, 28]. Finally, the (α,n) and (α,p) cross sections are practically insensitive to the choice of the GSF, leading to a χ^2 per experimental data point between 4.76 and 4.78 and an average deviation of 13.6% to 13.7% for the best-fit A-OMP, N-OMP, and LD, and an arbitrary choice of the GSF. This minor sensitivity to T_γ and the GSF is obvious from Eq. (2) where T_γ appears only as a minor contribution to the sum $\sum_i T_i$ in the denominator. Consequently, the following discussion provides detailed information on the sensitivities of the WFCFs (Sect. III A), the A-OMPs (Sect. III B), the N-OMPs (Sect. III C), and the LDs (Sect. III D), whereas a discussion of GSFs is omitted. The best-fit parameters (as stated above) will be used as a reference in the following presentation.

Fig. 1 illustrates the peculiar behavior of ^{38}Ar and the importance of the WFCF. The upper part (a) of Fig. 1 shows the total cross section $\sigma_{\rm reac}$ from the reference calculation and the compound-elastic $\sigma_{\rm compound}(\alpha,\alpha)$. Below the ($\alpha$,n) and ($\alpha$,p) thresholds, $\sigma_{\rm reac}$ is dominated by the compound-elastic contribution. And even up to almost 10 MeV, there is a significant compound-elastic contribution (blue dashed line) which is enhanced by the WFCF (in comparison to the calculation without WFCF, red dotted line). Note that the data for ^{38}Ar are shown as a function of $E_{\alpha,\rm lab}$ whereas the experiment [1] was performed in inverse kinematics.

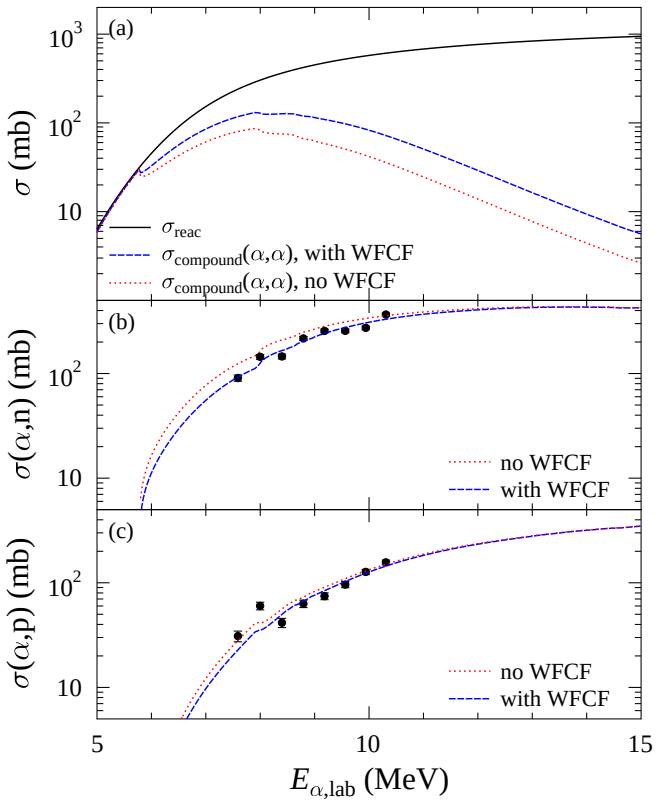

FIG. 1. (Color online) Total cross section $\sigma_{\rm reac}$ and compound-elastic $\sigma_{\rm compound}(\alpha,\alpha)$ for ^{38}Ar (upper, a), calculated without WFCF (dotted red) and with WFCF (dashed blue). Because of the increased $\sigma_{\rm compound}(\alpha,\alpha)$, the ($\alpha$,n) (middle, b) and ($\alpha$,p) (lower, c) cross sections are reduced by the WFCF. Further discussion see text.

The ^{38}Ar(α,n)^{41}Ca and ^{38}Ar(α,p)^{41}K cross sections are shown in the middle (b) and lower (c) parts of Fig. 1. Obviously, the reference calculation (including the WFCF) reproduces the new experimental data [1] very well, whereas a calculation without WFCF overestimates the (α,n) and (α,p) cross sections. Of course, the WFCF becomes most relevant for the energy range where the compound-elastic cross section has a significant contribution to the total reaction cross section $\sigma_{\rm reac}$ (i.e., below about 10 MeV). At the highest energies under study around 15 MeV, there is still a significant enhancement of $\sigma_{\rm compound}(\alpha,\alpha)$ by about a factor of two from the WFCF; however, here $\sigma_{\rm compound}(\alpha,\alpha)$ has only a very minor contribution of less than 1% to the total reaction cross section $\sigma_{\rm reac}$, and thus even a significant enhancement of $\sigma_{\rm compound}(\alpha,\alpha)$ does practically not affect the dominating (α,n) and (α,p) channels.

Next, the sensitivities to the different ingredients of the StM will be studied in detail for the ^{38}Ar(α,n)^{41}Ca and ^{38}Ar(α,p)^{41}K reactions. For better visibility, all plots will be normalized to the reference calculation with the smallest χ^2 (as defined above), and the same logarithmic scale is chosen for all plots of the ratio $r_{\rm calc} = \sigma_{\rm mod}/\sigma_{\rm ref}$ between the cross section with a modified parameter $\sigma_{\rm mod}$ and the reference cross section $\sigma_{\rm ref}$. In addition, also the new experimental data [1] are shown as ratio $r_{\rm exp} = \sigma_{\rm exp}/\sigma_{\rm ref}$. All Figs. 2 – 5 with the calculated sensitivities use the same scale with ratios r between 0.3 and 3.0; only in Fig. 3 the vertical size has been increased for better visibility because of the larger number of lines.

A. Width fluctuation correction factors

The WFCFs can be calculated in TALYS from three different models. Widely used are the approaches by Moldauer [29] and the iterative method by Hofmann *et al.* [30]. A more fundamental approach is based on the Gaussian orthogonal ensemble (GOE) of Hamiltonian matrices [31]; however, in practice this approach requires the calculation of triple integrals which leads to long computation times in particular at higher energies. It has been shown for neutron-induced reactions that the simpler Moldauer approach leads to almost identical results as the elaborate GOE approach [32, 33]. This has been verified for the α-induced reactions on ^{38}Ar in this study in coarse 1 MeV steps from 3 to 15 MeV. The difference between the Moldauer approach and the Hofmann approach remains small (see Fig. 2). Therefore, the TALYS default option by Moldauer was used for the reference calculation.

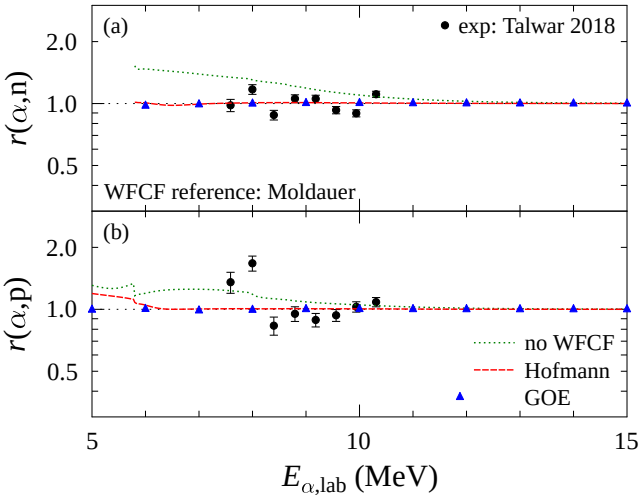

FIG. 2. (Color online) Sensitivity of the ^{38}Ar(α,n)^{41}Ca and ^{38}Ar(α,p)^{41}K reactions for different choices for the width fluctuation correction. All cross sections are normalized to the reference calculation (see text) which uses the Moldauer approach for the WFCFs. The deviation of the Hofmann approach (red dashed) is practically negligible, and also the GOE approach (blue points) does not show a major deviation from the reference calculation. However, the cross sections without width fluctuation correction are significantly higher below 10 MeV (green dash-dotted), in particular for the (α,n) channel.

For completeness it has to be mentioned that the TALYS default setting for the WFCFs is only active at

low energies. Above the separation energy of the projectile from the target, the WFCFs are assumed unity. Thus, for α-induced reactions on ^{38}Ar with $S_\alpha(^{38}\mathrm{Ar}) = 7.21$ MeV, the width fluctuation correction is turned off by default at $E_{\alpha,\mathrm{lab}} = 7.21$ MeV. It is obvious from Fig. 1 that this is not appropriate for the particular case of ^{38}Ar although this TALYS default setting is good for most other α-induced reactions. As a consequence, a TALYS calculation for $^{38}\mathrm{Ar} + \alpha$ with the default settings for the width fluctuation correction shows an unphysical kink at $E_{\alpha,\mathrm{lab}} = 7.21$ MeV ($E_{\mathrm{c.m.}} = 6.5$ MeV), see Fig. 5 of [1].

B. α-nucleus optical model potential

The A-OMP is the essential ingredient for the calculation of α-induced reaction cross sections. It defines the transmission $T_{\alpha,0}$ in the entrance channel in Eq. (2) which corresponds to the total reaction cross section σ_{reac}. There are 8 built-in options for the A-OMP in TALYS, and the recent ATOMKI-V1 potential has been implemented in addition. The results from the different AOMPs are shown in Fig. 3.

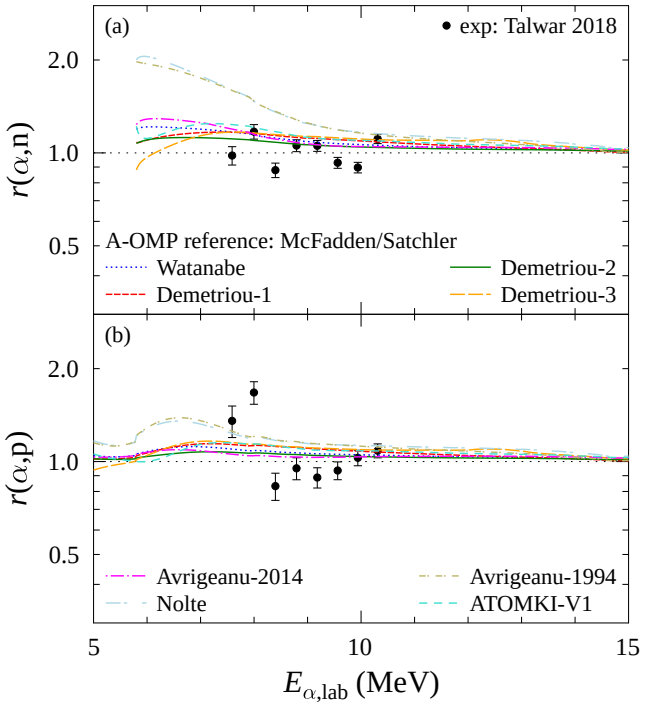

FIG. 3. (Color online) Same as Fig. 2 for the sensitivity of the ^{38}Ar(α,n)^{41}Ca and ^{38}Ar(α,p)^{41}K reactions on the chosen A-OMP. Except the early potentials by Nolte *et al.* [35] and Avrigenau *et al.* [36], the reproduction of the experimental data is quite good. But clearly the best description is obtained from the McFadden/Satchler potential [11].

As explained in [34], the calculated cross sections from different A-OMPs are very close to each other at higher energies. Differences become visible at lower energies below 10 MeV. The potentials by Nolte *et al.* [35] and the earlier version of Avrigeanu *et al.* [36] clearly overestimate in particular the (α,n) channel. As these potentials have been adjusted at higher energies, such a discrepancy at low energies is not surprising. Consequently, these potentials should not be used for the calculation of astrophysically relevant cross sections and reaction rates.

The potentials by Watanabe [37] (early TALYS default), Demetriou *et al.* [38] in three different versions, Avrigeanu *et al.* [39] in its recent version (new TALYS default), and ATOMKI-V1 [25] lead to (α,n) and (α,p) cross sections which remain relatively close to the reference calculation which is based on the simple 4-parameter potential by McFadden and Satchler [11]. However, contrary to the McFadden/Satchler potential, the other potentials show a trend to overestimate the (α,n) and (α,p) cross sections by about 10% to 30%, leading to a significantly worse χ^2 for the comparison with the new experimental data [1].

The present data confirm the general finding of [10] that the simple McFadden/Satchler potential does an excellent job at low energies in the $A \approx 20 - 50$ mass range. Furthermore, the variation of the calculated (α,n) and (α,p) cross sections from different A-OMPs is not as dramatic as for heavy target nuclei with masses above $A \approx 100$ where discrepancies exceeding one order of magnitude have been seen (e.g. [40]).

The calculation of astrophysical reaction rates for the ^{38}Ar(α,n)^{41}Ca and ^{38}Ar(α,p)^{41}K reactions is further hampered by the negative Q-value of both reactions, leading to numerical complications. This was already discussed in detail in [1], and it was concluded that the astrophysical reaction rate of both reactions has uncertainties which do not exceed a factor of two for all relevant temperatures. In the most relevant temperature range around $T_9 \approx 1$ (where T_9 is the temperature in GigaKelvin) the uncertainty of the reaction rates is about 30%.

C. Nucleon-nucleus optical model potential

The N-OMP essentially defines the branching ratio between the (α,n) and the (α,p) channel. However, the variation of the (α,n) and (α,p) cross sections remains relatively small because the major influence on the branching between (α,n) and (α,p) results from the available phase space. The results for the different N-OMPs under study are shown in Fig. 4.

The best description of the new experimental data is achieved by the TALYS default N-OMP by Koning and Delaroche [26]. Further N-OMPs in TALYS are based on the work of Jeukenne, Leujenne, and Mahaux (JLM) [41] in the version of Bauge *et al.* [42]. In addition to the original Bauge *et al.* potential, three modifications of the imaginary part of the JLM-type potential can be selected as suggested by Goriely and Delaroche [43].

In general, compared to the default Koning/Delaroche

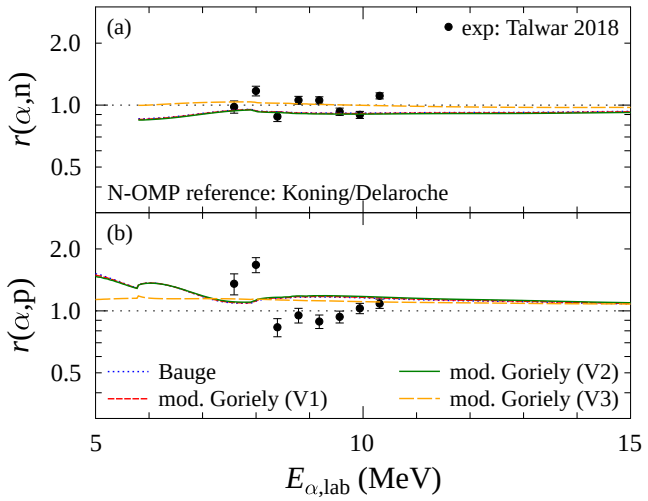

FIG. 4. (Color online) Same as Fig. 2 for the sensitivity of the ^{38}Ar(α,n)^{41}Ca and ^{38}Ar(α,p)^{41}K reactions on the chosen N-OMP. The JLM-type potentials show a trend to overestimate the (α,p) data and underestimate the (α,n) data.

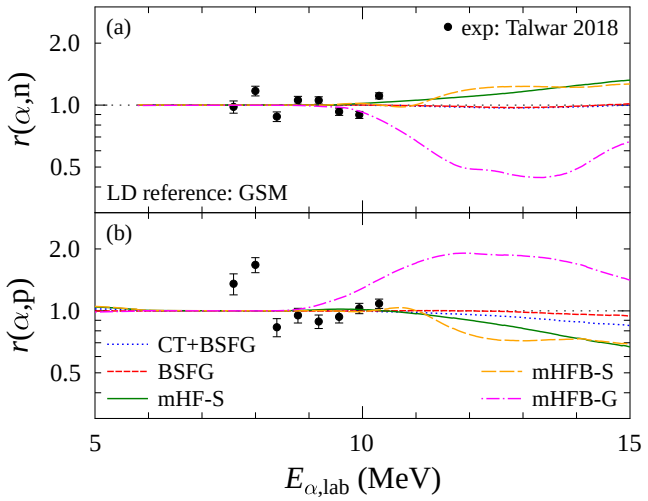

FIG. 5. (Color online) Same as Fig. 2 for the sensitivity of the ^{38}Ar(α,n)^{41}Ca and ^{38}Ar(α,p)^{41}K reactions on the chosen LD. The best-fit is obtained from the generalized superfluid model. At higher energies above 10 MeV, the mHFB-G LD which is based on Gogny forces, shows a much larger (α,p) cross section and lower (α,n) cross section than all other LDs. As expected, at low energies the role of the LD is very minor (see text).

potential, the JLM-type potentials overestimate the (α,p) channel and underestimate the (α,n) channel. An exception is the third modification of the JLM-type potentials where the imaginary strength is increased by a factor of two (so-called "*jlmmode 3*"). This increased imaginary potential favors the nucleon channels and reduces the compound-elastic contribution, leading to an overestimation of the (α,p) channel and a good description of the (α,n) channel.

D. Level density

As expected from the discussion around Eq. (3), the influence of the chosen LD on the calculated (α,n) and (α,p) cross sections is almost negligible at low energies. At these low energies all relevant levels in the residual nuclei are taken into account explicitly in the calculations. However, at higher energies the importance of the LD becomes visible (see Fig. 5).

The microscopic level density, calculated from a Gogny force [44], predicts much lower (α,n) cross sections above 10 MeV and higher (α,p) cross sections. The other available options behave close to the best-fit LD which is based on the generalized superfluid model [27, 28] (labeled "GSM") with a trend of slightly increased (α,n) and slightly decreased (α,p) cross sections. The other options are labeled by "CT+BSFG" for the constant-temperature model which is matched to the back-shifted Fermi gas model [45], "BSFG" for the back-shifted Fermi gas model [45, 46], "mHF-S" for microscopic Hartree-Fock using Skyrme forces [47], "mHFB-S" for microscopic Hartree-Fock-Bogoliubov using Skyrme forces [48], and "mHFB-G" for microscopic Hartree-Fock-Bogoliubov using Gogny forces [44].

E. Discussion

The calculation with the reference parameters is able to reproduce the new experimental data for the ^{38}Ar(α,n)^{41}Ca and ^{38}Ar(α,p)^{41}K reactions with a $\chi^2 \approx 4.8$ (per point) and an average deviation of about 14%. Obviously, it is not possible to reproduce the two (α,p) cross sections at the lowest energies which show significant enhancement over the otherwise smooth energy dependence. This enhancement most likely results from a resonant contribution which should be located around $E^* \approx 13.5$ MeV in ^{42}Ca with small J^π because of the enhanced decay to the (α,p) channel, i.e. towards ^{41}K (with low-J states at low excitation energies) and suppressed (α,n) contribution, i.e. towards ^{41}Ca with $J^\pi_{\text{g.s.}} = 7/2^-$.

The adjustment of the reference parameters via a strict χ^2 assessment clearly favors the A-OMP by McFadden and Satchler [11] in combination with the default N-OMP by Koning and Delaroche [26]. All other combinations of A-OMPs and N-OMPs lead to an increased χ^2 per point by at least 1.1 from its minimum value of about 4.8 to 5.9 and above. Contrary to this, the LD and the GSF are not well constrained by the new experimental data. For a well-defined choice of the LD, the available experimental data should be extended towards higher energies. The GSF could be best constrained by a measurement of the ^{38}Ar(α,γ)^{42}Ca cross section over a wide energy range.

In a next step, the reference parameters can be used to calculate α-induced cross sections for the mirror target nucleus ^{38}Ca and the neighboring argon isotopes ^{36}Ar and ^{40}Ar. As the essential parameters of the StM have

been adjusted to experimental data for ^{38}Ar, these calculations should be more reliable than earlier estimates from global parameter sets. Furthermore, the relevance of the width fluctuation correction will also be investigated for ^{38}Ca, ^{36}Ar, and ^{40}Ar.

IV. RESULTS FOR ^{38}CA, ^{36}AR, AND ^{40}AR

A. ^{38}Ca

The Q-values of the ^{38}Ca(α,n)^{41}Ti and ^{38}Ca(α,p)^{41}Sc reactions are $Q_n = -12.01$ MeV and $Q_p = +1.72$ MeV. Thus, proton emission from the ^{42}Ti compound nucleus dominates at low energies, and the compound-elastic channel is much weaker. Consequently, the width fluctuation correction is not relevant for these reactions. However, the residual nucleus ^{41}Sc of the ^{38}Ca(α,p)^{41}Sc reaction has only a very small proton separation energy of $S_p = 1.09$ MeV, and thus also the (α,2p) channel is open at all energies. According to TALYS, the (α,p) channel dominates below about 6 MeV whereas at higher energies the (α,2p) channel exceeds the (α,p) contribution. The (α,n) cross section remains below 1 mb up to 15 MeV. The results are shown in Fig. 6.

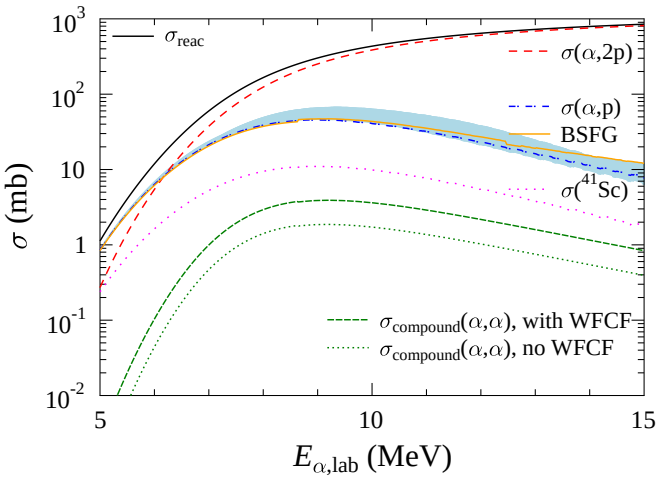

FIG. 6. (Color online) Total cross section σ_{reac} (full black line), compound-elastic $\sigma_{compound}(\alpha,\alpha)$ (green dashed and dotted), and ^{38}Ca(α,p)^{41}Sc (blue dash-dotted) and ^{38}Ca(α,2p)^{40}Ca (red long-dashed) reaction cross sections. The uncertainty of the ^{38}Ca(α,p)^{41}Sc cross section from the choice of different LDs is indicated by the blue shaded area. The dotted magenta line indicates the production cross section of ^{41}Sc, i.e. without contributions from higher-lying levels in the residual ^{41}Sc which decay preferentially by proton emission. The full orange line for the (α,p) cross section is calculated from the back-shifted Fermi gas LD and will be discussed later in Sect. IV C.

The calculation of the cross sections for ^{38}Ca uses the reference parameters which were fixed for ^{38}Ar (as explained above). Thus, the uncertainty of the predicted cross sections should be relatively low. As the LD was not well-constrained by the ^{38}Ar data, various parametrizations of the LD were used to estimate the resulting uncertainty for the ^{38}Ca(α,p)^{41}Sc cross section (blue-shaded area in Fig. 6).

As already mentioned above, the role of the width fluctuation correction remains minor. Similar to ^{38}Ar, the WFCF enhances the compound-elastic contribution by about a factor of two. However, because the compound-elastic channel is at least two orders of magnitude below the total cross section σ_{reac} for ^{38}Ca, the WFCF has practically no influence on the dominating (α,p) (at low energies) and (α,2p) channels (at higher energies above 6 MeV).

Because of the astrophysical relevance of (α,p) cross sections of $T_z = -1$ nuclei, the reference parameters are also used to calculate the astrophysical reaction rate $N_A\langle\sigma v\rangle$ for the ^{38}Ca(α,p)^{41}Sc reaction. The results are listed in Table I.

TABLE I. Astrophysical reaction rate $N_A\langle\sigma v\rangle$ of the ^{41}Sc production from the ^{38}Ca(α,p)^{41}Sc reaction, calculated from the ^{38}Ar reference parameters. The energy E_0 of the classical Gamow window is given to estimate the relevant energy range for the calculation of $N_A\langle\sigma v\rangle$.

T_9	$N_A\langle\sigma v\rangle$	E_0
–	(cm^3 s^{-1} mole^{-1})	(keV)
0.1	6.74×10^{-47}	472
0.2	1.80×10^{-32}	749
0.5	3.87×10^{-18}	1380
0.8	1.75×10^{-12}	1888
1.0	3.87×10^{-10}	2191
1.2	2.26×10^{-08}	2474
1.5	2.21×10^{-06}	2871
2.0	4.44×10^{-04}	3478
2.5	1.73×10^{-02}	4035
3.0	2.60×10^{-01}	4557

The calculation of the astrophysical reaction rate $N_A\langle\sigma v\rangle$ requires an additional consideration of the decay properties of all final states in the residual nucleus ^{41}Sc. The ^{41}Sc production cross section from the (α,p) reaction (as provided by TALYS) is composed essentially of the contributions of several low-lying states in ^{41}Sc which are taken into account explicitly, see Eq. (3). According to the ENSDF database [49, 50], only one excited state with $J^\pi = 7/2^+$ at $E^* = 2882$ keV has a noticeable branching to the $J^\pi = 7/2^-$ ground state of ^{41}Sc whereas the other excited states in ^{41}Sc decay preferentially by proton emission. Therefore the ^{41}Sc production cross section in TALYS has to be corrected accordingly; this leads to a slight reduction of the cross section in the astrophysically relevant energy region by less than a factor of two and a strong reduction at higher energies. The ^{41}Sc production cross section is shown in Fig. 6 as magenta dotted line.

The new recommended rate of the ^{41}Sc production

from the ^{38}Ca(α,p)^{41}Sc reaction is compared to previous calculations in Fig. 7. Significant discrepancies to all previous evaluations are found which result from the choice of the A-OMP, from the consideration of the preferential proton decay of excited states in ^{41}Sc, and from the numerical treatment.

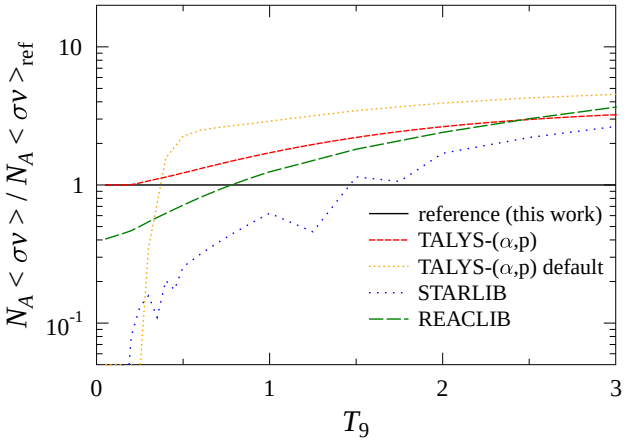

FIG. 7. (Color online) Astrophysical reaction rate $N_A\langle\sigma v\rangle$ of the ^{41}Sc production from the ^{38}Ca(α,p)^{41}Sc reaction: comparison of the new reference rate from the ^{38}Ar reference parameters to various previous calculations [24, 51, 52, 54–57]. For better visualization, all rates are normalized to the new reference rate $N_A\langle\sigma v\rangle_{\rm ref}$ from this work. Further discussion see text.

The relevance of the proton decay of excited states in ^{41}Sc is illustrated by the comparison with the rate which is calculated from the (α,p) cross section as provided by TALYS (red short-dashed line in Fig. 7, labeled "TALYS-(α,p)"). At very low temperatures below $T_9 \approx 0.3$, the Gamow window is located below 1 MeV. Because of the only slightly positive Q-value of $Q_p = +1.72$ MeV, excited states in the residual ^{41}Sc nucleus do not contribute in the ^{38}Ca(α,p)^{41}Sc reaction below $T_9 \approx 0.3$, and the rate is identical to the reference rate. Above $T_9 = 0.5$, the contributions of excited states increase and lead to an increased rate by about a factor of 1.7 at $T_9 = 1$ and more than a factor of 3 at $T_9 = 3$. Thus, the reference rate $N_A\langle\sigma v\rangle_{\rm ref}$ shows a different temperature dependence. Note that these rates were calculated numerically from the TALYS cross sections in small steps of 5 keV to avoid numerical complications at low temperatures. The numerical stability was checked carefully, see also the discussion in [1].

The role of different A-OMPs is illustrated by the TALYS default rate and by the rate in STARLIB [51, 52]. The TALYS default rate (orange dotted, "TALYS-(α,p) default" in Fig. 7) is based on the A-OMP by Watanabe which leads to increased cross sections by about a factor of two in the astrophysically relevant energy region around $T_9 = 1$. As the TALYS default calculation does not take into account the proton decay of excited states in ^{41}Sc, the influence of the A-OMP can be seen best by comparison to the "TALYS-(α,p)" curve in Fig. 7 which also neglects the proton decay of excited states in ^{41}Sc. The strong decrease of the TALYS default rate at low temperatures below $T_9 \approx 0.3$ results probably from numerics because TALYS automatically selects about 230 energies from 0 to 50 MeV to calculate $N_A\langle\sigma v\rangle$. (The TALYS default rate has been calculated within TALYS whereas the previously discussed rates have been calculated outside TALYS by numerical integration of TALYS cross sections in very small steps.)

Contrary to the TALYS default rate, the rate in STARLIB is based on the A-OMP by Demetriou *et al.* [38] in its third version [53]. This A-OMP typically shows lower cross sections than other A-OMPs at low energies. This trend to lower cross sections becomes also visible for the ^{38}Ar mirror nucleus at the lowest energies in Fig. 3 but very low energies are not accessible for ^{38}Ar because of the negative Q-values of the (α,n) and (α,p) reactions. The lower (α,p) cross sections from the Demetriou *et al.* A-OMP lead to lower reaction rates at low temperatures (blue dotted line in Fig. 7). At higher temperatures the Demetriou *et al.* rate exceeds the reference rate because proton emission from excited states in the ^{41}Sc residual nucleus was not taken into account. Similar to the TALYS default rate, also this rate shows was calculated within TALYS and shows a similar steep drop towards the lowest temperatures below $T_9 \approx 0.3$.

The REACLIB [54, 55] rate is taken from the NON-SMOKER calculations by Rauscher and Thielemann [56, 57]. NON-SMOKER uses the same A-OMP as the reference calculation in the present study, but does not take into account two-particle emission in the exit channel. This leads to an overestimation of the rate at higher temperatures because the dominating (α,2p) channel at higher energies is completely neglected (green dashed line in Fig. 7). At lower temperatures the REACLIB rate should approach the reference rate because the same A-OMP was used. The reason for the deviation by a factor of about 2 below $T_9 \approx 0.5$ is not clear; it may be related to the fact that REACLIB usually provides rates from their fit function instead of the underlying calculation.

Summarizing, the production rate $N_A\langle\sigma v\rangle$ of ^{41}Sc from the ^{38}Ca(α,p)^{41}Sc reaction in this work shows a different temperature dependence with lower rates at high temperatures because of the dominating proton decay of excited states in the residual ^{41}Sc nucleus. Around $T_9 \approx 1$, the choice of the reference A-OMP by McFadden/Satchler leads to a rate between the high rate from the TALYS default potential by Watanabe and the low rate from the Demetriou potential which was used for STARLIB. Because of these findings, further investigations of the (α,p) cross sections in the αp-process along isospin $T_z = -1$ nuclei are required to provide all (α,p) reaction rates in a consistent way and to reduce the uncertainties of the calculated (α,p) reaction rates.

B. ^{36}Ar

The nucleus ^{36}Ar is one of the two remaining outliers in the systematics of [10]. Unfortunately, there is only one experimental data point for the ^{36}Ar(α,p)^{39}K reaction which has been measured more than 60 years ago by Schwartz *et al.* [12].

The cross sections for ^{36}Ar have been calculated from the reference parameters of ^{38}Ar (as defined above) and are shown in Fig. 8. As for the other nuclei under study, the width fluctuation correction enhances the compound-elastic channel by about a factor of two. The compound-elastic contribution is smaller than in the ^{38}Ar case, but still significant. Consequently, there is a noticeable reduction of the ^{36}Ar(α,p)^{39}K cross section by about 25% around the energy of the experimental point at $E_{\alpha,\mathrm{lab}} = 7.4$ MeV. Although the reduction brings the calculation somewhat closer to the experimental data point, there still remains a huge discrepancy of at least one order of magnitude. As already pointed out in [10], the energy of the data point requires a correction by about -500 keV because $E_{\alpha,\mathrm{lab}} = 7.4$ MeV in [12] is the nominal beam energy without corrections for the energy loss in the entrance window of the target and in the target gas. But even this correction does not lead to reasonable agreement between the experiment and the present improved calculation. New experimental data are needed to confirm or to resolve the discrepancy between experiment on the one hand and calculation and systematics [10] on the other hand.

Similar to the ^{38}Ca case, the uncertainty of the ^{36}Ar(α,p)^{39}K cross section from the choice of the LD was investigated. It turns out that the level density in the residual nuclei is quite low, and thus the transmissions T_i in Eq. (3) are essentially defined by the sum over known low-lying levels in the first term on the l.h.s. of Eq. (3). Consequently, the choice of various LDs for the ^{36}Ar(α,p)^{39}K reaction leads to practically identical cross sections at low energies (within a line width in Fig. 8 below about 13 MeV). The range of calculations from different LDs is illustrated by the blue-shaded area in Fig. 8. A similar small sensitivity to the choice of the LD is found for the ^{36}Ar(α,n)^{39}Ca reaction.

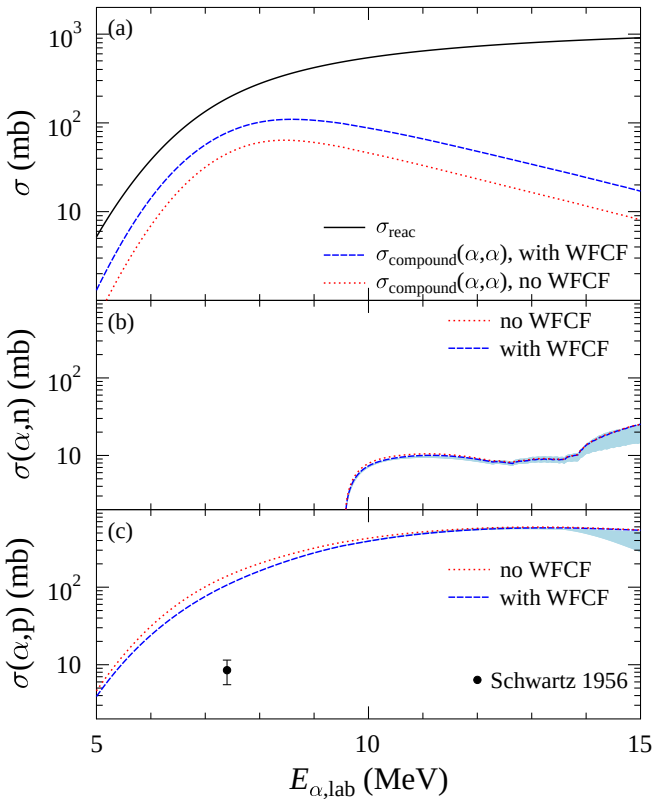

FIG. 8. (Color online) Total cross section σ_{reac} and compound-elastic $\sigma_{\mathrm{compound}}(\alpha,\alpha)$ for ^{36}Ar (upper, a), calculated from the reference parameters without WFCF (dotted red) and with WFCF (dashed blue). Because of the increased $\sigma_{\mathrm{compound}}(\alpha,\alpha)$, the ($\alpha$,n) (middle, b) and ($\alpha$,p) (lower, c) cross sections are slightly reduced by the WFCF. The minor sensitivity to the choice of the LD is illustrated by the blue-shaded areas. Further discussion see text.

C. ^{40}Ar

The procedure of the previous Sect. IV B was repeated for ^{40}Ar which is the second remaining outlier in the systematics of [10]. Again, the choice of the reference parameters in combination with a proper treatment of the WFCFs should lead to a reliable prediction of the ^{40}Ar(α,n)^{43}Ca and ^{40}Ar(α,p)^{43}K cross sections. The results are shown in Fig. 9 and compared to experimental data [12, 58, 59]. The (α,n) and (α,p) reactions have both slightly negative Q-values with $Q_n = -2.28$ MeV and $Q_p = -3.33$ MeV. In the shown energy range between 5 and 15 MeV, the (α,n) channel dominates and is very close to the total reaction cross section σ_{reac}. Again, the compound-elastic cross section is enhanced by about a factor of two, but this enhancement of the weak compound-elastic channel does practically not affect the stronger (α,n) and (α,p) channels, and thus the calculated reaction cross sections with and without WFCFs are practically identical.

As for ^{36}Ar, the early data by Schwartz *et al.* [12] are overestimated by almost one order of magnitude, and a significant overestimation persists also after a correction of the energy by about -500 keV (as for ^{36}Ar as discussed in the previous Sect. IV B and in [10]).

Interestingly, the later (α,p) data by Tanaka *et al.* [58] (only one data point below 15 MeV) and by Fenyvesi *et al.* [59] were also overestimated by the calculation in [10]. However, the present detailed study shows that the calculated ^{40}Ar(α,p)^{43}K cross section at higher energies depends sensitively on the chosen parametrization of the LD whereas the dominating ^{40}Ar(α,n)^{43}Ca cross section is only weakly affected. The range of calculated cross sections from different LDs is indicated in Fig. 9 as shaded area. The TALYS default level density which is based

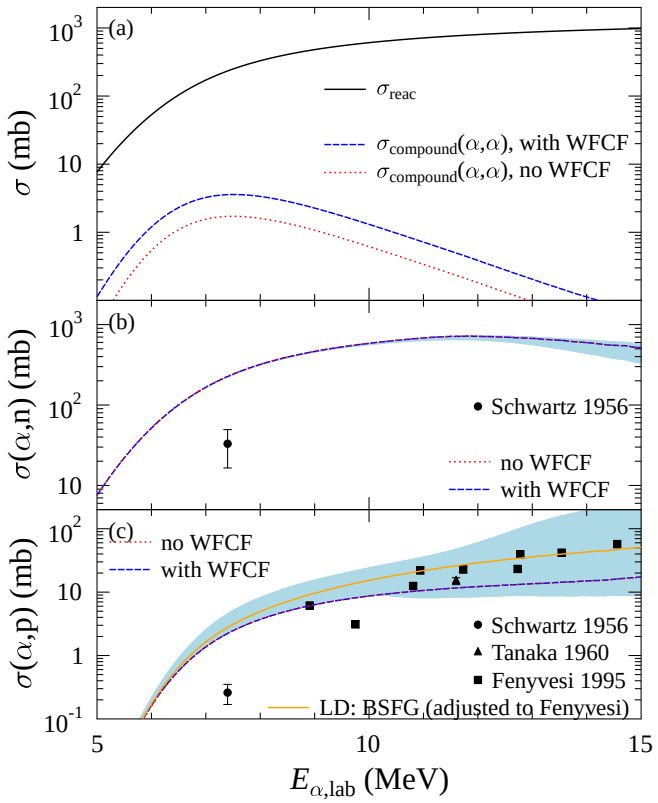

FIG. 9. (Color online) Total cross section σ_{reac} and compound-elastic $\sigma_{compound}(\alpha,\alpha)$ for ^{40}Ar (upper, a), calculated from the reference parameters without WFCF (dotted red) and with WFCF (dashed blue). The (α,n) and (α,p) cross sections are shown in the middle (b) and lower (c) parts. The range of calculations from different parametrizations of the LD is shown as lightblue shaded area. Whereas the (α,n) data are relatively insensitive to the choice of the LD, the description of the (α,p) data can be improved using a different LD. Further discussion see text.

on the constant temperature plus Fermi gas model (as used in [10]) leads to an overestimation of the experimental (α,p) data. Contrary to this, the reference LD from the generalized superfluid model slightly underestimates the experimental data, and the LD from the back-shifted Fermi gas (BSFG) model reproduces the experimental data well. Thus, it seems that at least for the residual odd-even nuclei with $A = 43$ the BSFG LD is a better choice than the reference LD from the generalized superfluid model.

Among the cross sections of the other nuclei ^{36}Ar, ^{38}Ar, and ^{38}Ca, only the ^{38}Ca(α,p)^{41}Sc cross section is slightly sensitive to the chosen LD. Therefore, those calculations were repeated using the BSFG LD instead of the reference LD from the generalized superfluid model. Below 10 MeV the calculated result from the BSFG LD is practically identical to the calculation with the reference LD, and above 10 MeV the BSFG LD leads to slightly higher cross sections (see orange line in Fig. 6).

If the final calculation of the ^{40}Ar(α,p)^{43}K cross section is considered as reliable in the entire energy range of Fig. 9, a correction factor for the early data by Schwartz *et al.* [12] can be derived. Assuming a 500 keV shift to lower energies because of the energy loss in the entrance window (as suggested in [10]), a correction factor of about 5 is found. The same correction procedure (500 keV energy shift and increase of the cross section by a factor of five) leads also to good agreement between the calculations and the experiment of Schwartz *et al.* [12] for the ^{40}Ar(α,n)^{43}Ca and ^{36}Ar(α,p)^{39}K reactions. This finding can be considered as evidence that such a correction is indeed required for the early Schwartz *et al.* data.

V. ISOSPIN CONSIDERATIONS

As pointed out in Sec. II C, the successful application of the StM is based on a sufficiently high level density in the compound nucleus, and thus the StM is applicable for intermediate mass and heavy nuclei. Under these circumstances the role of isospin conservation is very minor, and typical computer codes like TALYS do not consider isospin explicitly for the calculation of the transmission coefficients in Eq. (3). However, for light nuclei, in particular for target nuclei with isospin $T = 0$ ($N = Z$), substantial changes may occur for α-induced reactions. These changes are related to the fact that the α projectile with $T = 0$ can only populate states in the compound nucleus with the same isospin T as the target nucleus. Without explicit consideration of isospin, Eq. (3) overestimates the transmissions to the proton and neutron channels because of additional isospin couplings which result from $T \neq 0$ of the ejectiles. Contrary, the α channel with $T = 0$ is calculated correctly in Eq. (3). The resulting suppression of the (α,n) and (α,p) channels has been discussed in detail by Grimes [60], and Table I of [60] shows the isospin couplings for α-induced reactions on targets with isospin $T = 0, 1/2$, and 1. We follow the idea of [60], starting with the $T = 2$ target ^{40}Ar, and provide an approximate correction for the TALYS cross sections. Detailed information on the role of isospin in StM calculations for nuclear astrophysics is also provided in [61, 62]; in particular, [62] focuses on the important point of isospin suppression in (α,γ) capture reactions in self-conjugate $N = Z$ nuclei.

A. Target ^{40}Ar, compound ^{44}Ca: $T = 2$, $T_z = +2$

According to [60], the isospin coupling is given by the square of the respective Clebsch-Gordan coefficient which couples the isospins T_E of the ejectile and T_R of the residual nucleus to the isospin T_C of the compound nucleus. For the ^{40}Ar target we find for the α channel $< T_R\, T_{z,R}\; T_E\, T_{z,E} \,|\, T_C\, T_{z,C} >= 1.0$; the coupling to the α channel is 1.0 (this result also holds for all reactions under study). For the proton channel with the residual ^{43}K ($T_R = 5/2$, $T_{z,R} = +5/2$) we obtain a Clebsch-Gordan

coefficient of $\sqrt{5/6}$, leading to a coupling of 5/6. For the neutron channel with the residual ^{43}Ca ($T_R = 3/2$, $T_{z,R} = +3/2$) the coupling is 1.0; contributions of higher-lying states in ^{43}Ca with $T_R = 5/2$; $T_{z,R} = +3/2$ with a coupling of 1/6 are neglected. The given couplings extend Table I of [60] for the case of $T_C = 2$, $T_{z,C} = +2$.

An approximate correction to the TALYS calculations in the previous sections can be made as follows. The correction is based on the assumptions of isospin conservation (also excluding isospin mixing) and the independence of the transmission coefficients on the isospin. It will be shown that the resulting corrections are minor for the reactions under study, and thus the above simplifying assumptions have no major effect on the final conclusions of the present study. Furthermore, as isospin conservation is violated to some extent, the following correction may be considered as an upper limit for the relevance of isospin in the StM.

The isospin-corrected cross sections $\sigma_{\rm iso}(\alpha, X)$ are given by

$$\sigma_{\rm iso}(\alpha, X) = \mathcal{N}\, w_X\, \sigma(\alpha, X) \tag{5}$$

where the w_X are the isospin couplings (as provided above and in Table I of [60]), and $\mathcal{N}$ is a normalization factor to fulfill

$$\begin{aligned}\sigma_{\rm reac} &\approx \sigma(\alpha,{\rm n}) + \sigma(\alpha,{\rm p}) + \sigma(\alpha,\alpha) \\ &\approx \sigma_{\rm iso}(\alpha,{\rm n}) + \sigma_{\rm iso}(\alpha,{\rm p}) + \sigma_{\rm iso}(\alpha,\alpha)\end{aligned} \tag{6}$$

for the total α-induced reaction cross section $\sigma_{\rm reac}$ at low energies; other open channels like e.g. (α,γ) are typically weak and are neglected in Eq. (6). For ^{40}Ar this results in

$$\mathcal{N} = \left[1 - \frac{\sigma(\alpha,{\rm p})}{6\,\sigma_{\rm reac}}\right]^{-1} \tag{7}$$

from $w_{\rm p} = 5/6$ and $w_{\rm n} = w_\alpha = 1$. Note that $\mathcal{N} \geq 1$ close to unity, thus leading to an enhancement of the reaction channels with $w_X = 1$ and to a reduction for channels with $w_X < 1$. Because the (α,p) contribution to $\sigma_{\rm reac}$ does not exceed a few per cent in the energy range under study (see Fig. 9), the normalization factor $\mathcal{N}$ in Eq. (7) remains very close to unity for ^{40}Ar. According to Eq. (5), the (α,p) cross section is thus reduced by about a factor of 5/6 which is inside the shown uncertainty from the choice of the level density, and the other channels are practically not affected by the isospin correction.

B. Target ^{38}Ar, compound ^{42}Ca: $T = 1$, $T_z = +1$

The respective numbers for the couplings are $w_{\rm p} = 3/4$ and $w_{\rm n} = w_\alpha = 1$, and the normalization is given by

$$\mathcal{N} = \left[1 - \frac{\sigma(\alpha,{\rm p})}{4\,\sigma_{\rm reac}}\right]^{-1} \tag{8}$$

As the (α,p) contribution remains below 40% for the whole energy range under study, the normalization factor does not exceed $\mathcal{N} \approx 1.1$, leading only to a slight enhancement of the (α,n) and (α,α) channels and a reduction of the (α,p) cross section by about 20%.

In Sec. III C and Fig. 4 it was pointed out that the branching between the (α,n) and (α,p) channels depends essentially on the chosen N-OMP, and it was concluded that only the TALYS default N-OMP by Koning and Delaroche [26] is able to reproduce the new experimental data [1]. The JLM-type potentials showed a trend to overestimate the (α,p) cross sections and underestimate the (α,n) cross sections. These deviations of the JLM-type potentials are approximately compensated by the isospin corrections from Eq. (5), and thus the clear preference for the TALYS default potential by Koning and Delaroche [26] is weakened by the isospin correction in Eq. (5).

C. Target ^{38}Ca, compound ^{42}Ti: $T = 1$, $T_z = -1$

Here the results for w_X and $\mathcal{N}$ can be taken from the previous Sec. V B; only the role of neutrons and protons has to be exchanged in the given numbers for $\mathcal{N}$ and w_X. Because of the strongly negative Q-value of $Q_n \approx -12$ MeV, the isospin corrections vanish for almost the full energy range under study. In particular, the calculated reaction rates in Table I are not affected by the isospin correction.

D. Target ^{36}Ar, compound ^{40}Ca: $T = 0$, $T_z = 0$

As already pointed out in [60], the largest corrections are expected for α-induced reactions on $N = Z$ target nuclei with $T = 0$. Here we find $w_{\rm n} = w_{\rm p} = 1/2$, $w_\alpha = 1.0$, and

$$\mathcal{N} = \left[1 - \frac{\sigma(\alpha,{\rm n}) + \sigma(\alpha,{\rm p})}{2\,\sigma_{\rm reac}}\right]^{-1} \tag{9}$$

which leads to an enhancement of the α channel and to a reduction of the (α,n) and (α,p) cross sections. However, the reduction does not reach a factor of two (as one might expect from the coupling of 1/2 for the neutron and proton channels) because the total reaction cross section is dominated by the (α,p) contribution. Note that in the extreme case of $\sigma_{\rm reac} \approx \sigma(\alpha,{\rm p})$, the normalization approaches $\mathcal{N} \approx 2$, thus compensating the reduction by the coupling of 1/2 in Eq. (5); in this case the strong enhancement of the tiny (α,α) contribution by a factor of two does practically not affect the dominating (α,p) channel.

The isospin-corrected cross sections for ^{36}Ar are shown in Fig. 10. It is obvious from Fig. 10 that the reduction of the ^{36}Ar(α,p)^{39}K cross section from the isospin correction in Eq. (5) is only about 30% at 7.5 MeV and thus

cannot resolve the huge discrepancy to the experimental data point by Schwartz *et al.* [12].

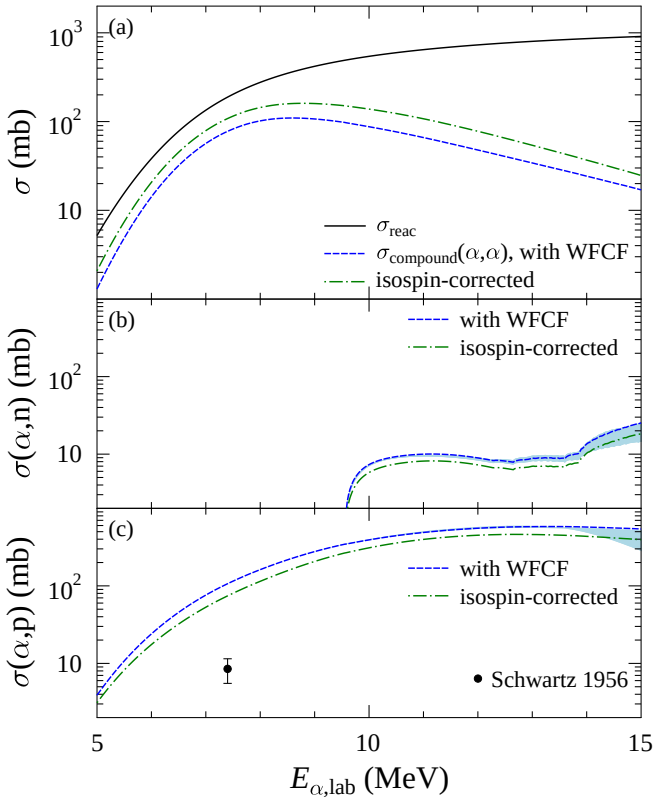

FIG. 10. (Color online) Same as Fig. 8, but with isospin correction: Total cross section σ_{reac} and compound-elastic $\sigma_{compound}(\alpha,\alpha)$ for ^{36}Ar (upper, a), calculated from the reference parameters with width fluctuation correction (dashed blue) and with additional isospin correction (dash-dotted green) from Eq. (5). The isospin correction leads to an increased $\sigma_{compound}(\alpha,\alpha)$, and it reduces the ($\alpha$,n) (middle, b) and ($\alpha$,p) (lower, c) cross sections by about 30%.

VI. CONCLUSIONS

The new experimental data for the ^{38}Ar(α,n)^{41}Ca and ^{38}Ar(α,p)^{41}K reactions [1] were analyzed within the statistical model using the TALYS code. Best-fit input parameters for the statistical model calculations were determined by a χ^2-based assessment [1]. The present study provides a careful discussion of the uncertainties from the different ingredients of the statistical model. It is found that a very good description of the experimental data can only be achieved from the α-nucleus potential by McFadden and Satchler [11] in combination with the default nucleon potential by Koning and Delaroche [26]. The smallest χ^2 is furthermore achieved for the level density from the generalized superfluid model, but because of the minor sensitivity to the level density, other parametrizations of the level density are not excluded by the new data. As the experimental (α,n) and (α,p) data for ^{38}Ar are not sensitive to the chosen γ-ray strength, no conclusion can be drawn on the choice of the γ-ray strength function. In addition, the importance of a proper treatment of the width fluctuation correction is pointed out especially for the ^{38}Ar(α,n)^{41}Ca and ^{38}Ar(α,p)^{41}K reactions. Isospin corrections to the calculated reaction cross sections reduce the ^{36}Ar(α,n)^{39}Ca and ^{36}Ar(α,p)^{39}K cross sections by about 30%, play a minor role with about $10-20$% correction for ^{38}Ar, and are practically negligible for ^{38}Ca and ^{40}Ar.

The best-fit parameters from the ^{38}Ar data are used as reference parameters to predict α-induced cross sections for the isospin mirror nucleus ^{38}Ca and for the neighboring argon isotopes ^{36}Ar and ^{40}Ar with improved reliability, and a new astrophysical reaction rate $N_A\langle\sigma v\rangle$ is calculated for the ^{38}Ca(α,p)^{41}Sc reaction. This new $N_A\langle\sigma v\rangle$ shows a different temperature dependence than previous calculations because proton decay from excited states in the residual ^{41}Sc nucleus was not taken into account in earlier work. However, before firm conclusions on astrophysical consequences can be drawn, further (α,p) reactions on the isospin $T_z = -1$ nuclei from ^{22}Mg to ^{34}Ar should also be re-investigated.

For ^{36}Ar the disagreement between the early experimental data by Schwartz *et al.* [12] for the ^{36}Ar(α,p)^{39}K reaction persists, and this holds also for the ^{40}Ar(α,n)^{43}Ca and ^{40}Ar(α,p)^{43}K reactions. But it was found that more recent data for the ^{40}Ar(α,p)^{43}K reaction [58, 59] can now be reproduced in a calculation which uses the well-constrained reference parameters for the α-nucleus potential and the nucleon-nucleus potential and a different level density from the back-shifted Fermi gas model. ^{36}Ar and ^{40}Ar have been identified as the two remaining outliers in the general systematics of α-induced cross sections in the $A \approx 20-50$ mass range [10]. At least for ^{40}Ar, the role as outlier is reduced by the improved reproduction of ^{40}Ar(α,p)^{43}K data of [58, 59]. In combination with the good description of the new data for ^{38}Ar, the α-induced cross sections for ^{36}Ar and ^{40}Ar may also be considered as regular if all early data by Schwartz *et al.* [12] for ^{36}Ar and ^{40}Ar are shifted by about 500 keV to lower energies and increased by about a factor of five.

ACKNOWLEDGMENTS

We thank Ernst Rehm for encouraging discussions, Stephane Goriely and Christian Iliadis for additional information on the STARLIB database, Arjan Koning for his help with TALYS, and the anonymous referee for pointing to the relevance of isospin in statistical model calculations. This work was supported by NKFIH (K108459 and K120666) and U.S. Department of Energy, Office of Science, Office of Nuclear Physics, under Contract No. DE-AC02-06CH11357.

[1] R. Talwar, M. J. Bojazi, P. Mohr, K. Auranen, M. L. Avila, A. D. Ayangeakaa, J. Harker, C. R. Hoffman, C. L. Jiang, S. A. Kuvin *et al.*, Phys. Rev. C **97**, 055801 (2018).

[2] D. Kahl, H. Yamaguchi, S. Kubono, A. A. Chen, A. Parikh, D. N. Binh, J. Chen, S. Cherubini, N. N. Duy, T. Hashimoto *et al.*, Phys. Rev. C **97**, 015802 (2018).

[3] A. M. Long, T. Adachi, M. Beard, G. P. A. Berg, M. Couder, R. J. deBoer, M. Dozono, J. Görres, H. Fujita, Y. Fujita *et al.*, Phys. Rev. C **97**, 054613 (2018).

[4] A. M. Long, T. Adachi, M. Beard, G. P. A. Berg, Z. Buthelezi, J. Carter, M. Couder, R. J. deBoer, R. W. Fearick, S. V. Förtsch *et al.*, Phys. Rev. C **95**, 055803 (2017).

[5] K. Schmidt, Nuclear Physics in Astrophysics NPA-VIII, Catania, 18-23 June 2017, oral presentation.

[6] R. K. Wallace and S. E. Woosley, Astroph. J. Suppl. **45**, 389 (1981).

[7] H. Schatz and K. E. Rehm, Nucl. Phys. **A777**, 601 (2006).

[8] A. Parikh, J. José, G. Sala, C. Iliadis, Prog. Part. Nucl. Phys. **69**, 225 (2013).

[9] S. O'Brien, T. Adachi, G. P. A. Berg, M. Couder, M. Dozono, H. Fujita, Y. Fujita, J. Görres, K. Hatanaka, D. Ishikawa *et al.*, AIP Conf. Proc. **1090**, 288 (2009).

[10] P. Mohr, Europ. Phys. J. **51**, 56 (2015).

[11] L. McFadden and G. R. Satchler, Nucl. Phys. **84**, 177 (1966).

[12] R. B. Schwartz, J. W. Corbett, W. W. Watson, Phys. Rev. **101**, 1370 (1956).

[13] M. L. Avila, K. E. Rehm, S. Almaraz-Calderon, A. D. Ayangeakaa, C. Dickerson, C. R. Hoffman, C. L. Jiang, B. P. Kay, J. Lai, O. Nusair *et al.*, Phys. Rev. C **94**, 065804 (2016).

[14] A. M. Howard, M. Munch, H. O. U. Fynbo, O. S. Kirsebom, K. L. Laursen, C. Aa. Diget, N. J. Hubbard, Phys. Rev. Lett. **115**, 052701 (2015).

[15] J. R. Tomlinson, J. Fallis, A. M. Laird, S. P. Fox, C. Akers, M. Alcorta, M. A. Bentley, G. Christian, B. Davids, T. Davinson *et al.*, Phys. Rev. Lett. **115**, 052702 (2015).

[16] T. Anderson, M. Skulski, A. Clark, A. Nelson, K. Ostdiek, Ph. Collon, G. Chmiel, T. Woodruff, M. Caffee, Phys. Rev. C **96**, 015803 (2017).

[17] P. Mohr, Phys. Rev. C **89**, 058801 (2014).

[18] S. Almaraz-Calderon, P. F. Bertone, M. Alcorta, M. Albers, C. M. Deibel, C. R. Hoffman, C. L. Jiang, S. T. Marley, K. E. Rehm, C. Ugalde, Phys. Rev. Lett. **112**, 152701 (2014); Erratum Phys. Rev. Lett. **115**, 179901(E) (2015).

[19] M. Bowers, Y. Kashiv, W. Bauder, M. Beard, P. Collon, W. Lu, K. Ostdiek, D. Robertson, Phys. Rev. C **88**, 065802 (2013).

[20] W. Hauser and H. Feshbach, Phys. Rev. **87**, 366 (1952).

[21] T. Rauscher, Int. J. Mod. Phys. E **20**, 1071 (2011).

[22] T. Rauscher, Astroph. J. Suppl. **201**, 26 (2012).

[23] P. Mohr, Gy. Gyürky, Zs. Fülöp, Phys. Rev. C **95**, 015807 (2017).

[24] A. J. Koning, S. Hilaire, S. Goriely, computer code TALYS, version 1.8, *http://www.talys.eu*.

[25] P. Mohr, G. G. Kiss, Zs. Fülöp, D. Galaviz, Gy. Gyürky, E. Somorjai, At. Data Nucl. Data Tables **99**, 651 (2013).

[26] A. J. Koning and J. P. Delaroche, Nucl. Phys. **A713**, 231 (2003).

[27] A. V. Ignatyuk, K. K. Istekov, G. N. Smirenkin, Sov. J. Nucl. Phys. **29**, 450 (1979).

[28] A. V. Ignatyuk, J. L. Weil, S. Raman, S. Kahane, Phys. Rev. C **47**, 1504 (1993).

[29] P. A. Moldauer, Phys. Rev. C **14**, 764 (1976).

[30] H. M. Hofmann, J. Richert, J. W. Tepel, H. A. Weidenmüller, Ann. Phys. **90**, 403 (1975).

[31] J. J. M. Verbaarschot, H. A. Weidenmüller, M. R. Zirnbauer, Phys. Rep. **129**, 367 (1985).

[32] S. Hilaire, Ch. Lagrange, A. J. Koning, Ann. Phys. **306**, 209 (2003).

[33] T. Kawano, R. Capote, S. Hilaire, P. Chau Huu-Tai, Phys. Rev. C **94**, 014612 (2016).

[34] P. Mohr, Phys. Rev. C **87**, 035802 (2013).

[35] M. Nolte, H. Machner, J. Bojowald, Phys. Rev. C **36**, 1312 (1987).

[36] V. Avrigeanu, P. E. Hodgson, M. Avrigeanu, Phys. Rev. C **49**, 2136 (1994).

[37] S. Watanabe, Nucl. Phys. **8**, 484 (1958).

[38] P. Demetriou, C. Grama, and S. Goriely, Nucl. Phys. **A707**, 253 (2002).

[39] V. Avrigeanu, M. Avrigeanu, C. Mănăilescu, Phys. Rev. C **90**, 044612 (2014).

[40] E. Somorjai, Zs. Fülöp, A. Z. Kiss, C. E. Rolfs, H.-P. Trautvetter, U. Greife, M. Junker, S. Goriely, M. Arnould, M. Rayet, T. Rauscher, H. Oberhummer, Astron. Astrophys. **333**, 1112 (1998).

[41] J.-P. Jeukenne, A. Lejeune, C. Mahaux, Phys. Rev. C **16**, 80 (1977).

[42] E. Bauge, J. P. Delaroche, M. Girod, Phys. Rev. C **63**, 024607 (2001).

[43] S. Goriely and J.-P. Delaroche, Phys. Lett. B **653**, 178 (2007).

[44] S. Hilaire, M. Girod, S. Goriely, A. J. Koning, Phys. Rev. C **86**, 064317 (2012).

[45] A. Gilbert and A. Cameron, Can. J. Phys. **43**, 1446 (1965).

[46] W. Dilg, W. Schantl, H. Vonach, M. Uhl, Nucl. Phys. **A217**, 269 (1973).

[47] S. Goriely, F. Tondeur, J. Pearson, At. Data Nucl. Data Tables **77**, 311 (2001).

[48] S. Goriely, S. Hilaire, A. J. Koning, Phys. Rev. C **78**, 064307 (2008).

[49] Online database ENSDF, *http://www.nndc.bnl.gov/ensdf*.

[50] C. D. Nesaraja and E. A. Mccutchan, Nucl. Data Sheets **133**, 1 (2016).

[51] Reaction rate database STARLIB, V6.5, 09-06-2017, *https://starlib.github.io/Rate-Library/*.

[52] A. L. Sallaska, C. Iliadis, A. E. Champagne, S. Goriely, S. Starrfield, F. X. Timmes, Astrophys. J. Suppl. **207**, 18 (2013).

[53] S. Goriely, private communication.

[54] Reaction rate database REACLIB, version 2.0, *https://groups.nscl.msu.edu/jina/reaclib/db/*.

[55] R. H. Cyburt, A. M. Amthor, R. Ferguson, Z. Meisel, K. Smith, S. Warren, A. Heger, R. D. Hoffman, T. Rauscher *et al.*, Astrophys. J. Suppl. **189**, 240 (2010).

[56] T. Rauscher, computer code NON-SMOKER, *http://nucastro.org/websmoker.html*.
[57] T. Rauscher and F.-K. Thielemann, At. Data Nucl. Data Tables **75**, 1 (2000).
[58] S. Tanaka, M. Furukawa, T. Mikumo, S. Iwata, M. Yagi, H. Amano, J. Phys. Sco. Japan **15**, 952 (1960).
[59] A. Fenyvesi, F. Tárkányi, F. Szelecsényi, T. Takács, Z. Szücs, T. Molnár, S. Sudár, Appl. Rad. Isot. **46**, 1413 (1995).
[60] S. M. Grimes, Phys. Rev. C **46**, 1064 (1992).
[61] T. Rauscher and F.-K. Thielemann, Proc. *2nd Oak Ridge Symposium on Atomic and Nuclear Astrophysics*, Oak Ridge, Tennessee, December 02-06, 1997, Ed. A. Mezzacappa, IoP Publishing, Bristol, UK, 1998, p. 519.
[62] T. Rauscher, F.-K. Thielemann, J. Görres, M. Wiescher, Nucl. Phys. **A675**, 695 (2000).